

Supporting information to

**Self-standing sulfur cathodes enabled by single Fe sites decorated
fibrous membrane for durable lithium-sulfur batteries**

Gang Zhao,^{1,+} Qiuji Chen,^{2,3+} Lei Wang,¹ Tianran Yan,¹ Hongtai Li,¹ Cheng Yuan,¹ Jing Mao,⁴

Xuefei Feng,⁵ Dan Sun,^{2,3*} Liang Zhang^{1,*}

1. Institute of Functional Nano & Soft Materials (FUNSOM), Jiangsu Key Laboratory for Carbon-Based Functional Materials & Devices, Soochow University, 199 Ren'ai Road, Suzhou 215123, China
2. CAS Key Laboratory of Design and Assembly of Functional Nanostructures, Fujian Key Laboratory of Nanomaterials, Fujian Institute of Research on the Structure of Matter, Chinese Academy of Sciences, Fuzhou, 350002 China
3. Xiamen Key Laboratory of Rare Earth Photoelectric Functional Materials, Xiamen Institute of Rare Earth Materials, Haixi Institutes, Chinese Academy of Sciences, Xiamen, 361021 China
4. School of Materials Science and Engineering, Zhengzhou University, Zhengzhou 450001, China
5. National Synchrotron Radiation Laboratory, University of Science and Technology of China, Hefei 230026, China

+These two authors contributed equally to this work.

*Email: liangzhang2019@suda.edu.cn (Liang Zhang); xmsundan@fjirsm.ac.cn (Dan Sun)

Experimental Section

Preparation of Fe-ZIF8 nanocrystals

In a typical procedure, 3.94 g of 2-methylimidazole (purity >98.0%, Aladdin) was dissolved in 300 mL of methanol (purity >99.5%, Jiangsu Qiangsheng Chemical Reagent) to form a clear solution and then mixed with 300 mL of methanol solution containing 3.39 g of $\text{Zn}(\text{NO}_3)_2 \cdot 6\text{H}_2\text{O}$ (purity >98%, Sinopharm Chemical Reagent) and 100 mg of $\text{Fe}(\text{NO}_3)_3 \cdot 9\text{H}_2\text{O}$ (purity >99%, Energy Chemical Reagent). After vigorous stirring at 60°C for 24 h, the resulting precipitate was collected by centrifugation and washed by methanol for three times. After drying in vacuum at 60 °C for 12 h, the final product with pale yellow color was obtained. Bare ZIF8 nanocrystal was prepared by a similar procedure except for the addition of $\text{Fe}(\text{NO}_3)_3 \cdot 9\text{H}_2\text{O}$.

Preparation of FeSA-PCNF

1.05 g of synthesized Fe-ZIF8 was dispersed in 8 mL of dimethylformamide (DMF; purity >99.5%, Aladdin) by sonication for 1 h, followed by the addition of 0.7 g of polyacrylonitrile (PAN; M.W. ~150 000; Sigma-Aldrich) and 0.175 g of polyvinylpyrrolidone (PVP; M.W. ~1 300 000; Macklin). The mixture was stirred for 24 h and then transferred into a plastic syringe with a 20-gauge blunt tip needle for electrospinning. The distance between the tip of needle and aluminum foil collector was 15 cm, and the feeding rate of the spinning solution was 1 ml h⁻¹. The applied positive voltage was set at 14 kV. The obtained fibrous membrane was pre-oxidized in air at 260 °C for 2 h and then carbonized at 950 °C for 2 h in an N₂ atmosphere with a heating rate of 5 °C min⁻¹ to obtain FeSA-PCNF. For comparison, PCNF was obtained by substituting Fe-ZIF8 with ZIF8 in the electrospinning solution. CNF was prepared by the calcination of pure PAN fibers. Fe-N-C was prepared by directly calcination of Fe-ZIF8.

Characterization of the materials

The morphologies were characterized by scanning electron microscopy (SEM, G500 ZEISS). The internal structure and high-resolution lattice were measured by transmission electron microscopy (TEM, 200X, Talos) equipped with energy dispersive X-ray spectrometer (EDS). X-ray diffraction (XRD) with Cu K α radiation was performed at Empyrean in the range of $2\theta = 5-90^\circ$. UV-vis spectroscopy was performed using UV-vis spectrophotometer (PE750). The Raman spectroscopy was recorded by the Raman spectrometer (Horiba HR800) with a 633 nm laser. The N₂ adsorption/desorption isotherm was measured on a Micromeritics ASAP 2460 to analyze the specific surface area, pore volume, and pore size distribution. The Fe concentration was conducted on the inductively coupled plasma atomic emission spectroscopy (ICP-AES). The Fe K-edge X-ray absorption fine structure (XAFS) measurement was performed at beamline 1W1B of Beijing Synchrotron Radiation Facility (BSRF) and beamline 11B of Shanghai Synchrotron Radiation Facility (SSRF). For the ex-situ characterizations, standard procedures were used to handle samples, including the disassembly, rinse, and transfer. The electrodes at different states of charge were disassembled in the Ar filled glovebox (H₂O < 0.1ppm, O₂ < 0.1ppm) and rinsed with DME solution thoroughly to remove the surface residue. Then the electrodes were sealed with kapton films for the XAFS measurement to avoid the change of charge states. The analysis of XAFS data was performed using the Athena software in Demeter package.

Polysulfide absorption test

The Li₂S₆ solution (2 mM) was prepared by dissolving sulfur and lithium sulfide (Li₂S; purity >99.9%; Alfa) in the 1,2-dimethoxyethane (DME; purity >99.99%; Aladdin) solvent with a molar ratio of 5:1, and then vigorous stirring for 24 h at 60 °C. Then 10 mg of FeSA-PCNF, PCNF and CNF powders were dispersed in 2 ml Li₂S₆ solution, respectively. After soaking for certain time, the supernatant was absorbed for UV-vis test and drop onto the carbon-coated aluminum foil for XPS test.

Assembly of Li-S batteries and electrochemical measurements

The obtained fibrous membrane was cut into discs with a diameter of 12 mm which were directly used as the self-standing cathode. The CR2032-type coin cells were assembled using lithium foil with diameter of 16 mm as anode and Celgard 2500 as separator in Ar-filled glovebox ($O_2 < 0.1$ ppm, $H_2O < 0.1$ ppm). The electrolyte consists of 1 M bis (trifluoromethane sulfonyl) imide (LiTFSI) in 1, 2-dimethoxyethane (DME) and 1, 3-dioxolane (DOL) (1:1 in volume) with 2.0 wt% $LiNO_3$ as additive. The 1 M Li_2S_6 -contained electrolyte was used as catholyte (10 μ l of catholyte equals to 1.92 mg sulfur), while certain amount of additional bare electrolyte was added to regulate the electrolyte-to-sulfur (E/S) ratio. Typically, 10 μ l of catholyte and 40 μ l of additional bare electrolyte with an areal sulfur loading of 1.7 mg cm^{-2} were used for rate performance and cyclability tests. For high sulfur loading tests, 25, 50 and 100 μ l of catholyte were used to achieve the sulfur loading of 4.3, 8.5 and 17 mg cm^{-2} , respectively. The galvanostatic charge-discharge test was measured by the Land CT2001A battery test system. CHI660E electrochemical workstation was used for CV test and the scan rate was from 1 to 5 $mV s^{-1}$ in the voltage of 1.7 to 2.8 V. Electrochemical impedance spectroscopy was measured in the frequency range of 10 mHz to 100 kHz.

The nucleation and dissolution of Li_2S measurements

0.2 M Li_2S_8 solution was prepared by mixing sulfur and Li_2S in tetraglyme (TEGDME; purity >99.5%; Macklin) solvent with a molar ratio of 7:1. The FeSA-PCNF, PCNF and CNF carbon matrix were directly used as self-standing cathodes and lithium foil is used as the anode, with 15 μ l of 0.2 M Li_2S_8 solution as active materials. The assembled batteries were galvanostatically discharged to 2.06 V at a current of 0.112 mA and then potentiostatically discharged to 2.05 V until the discharged current was below 0.01 mA. Similarly, the batteries were assembled using the

same electrode material and electrolyte. The batteries were first galvanostatically discharged to 1.7 V at a current of 0.112 mA and then galvanostatically discharged to 1.8 V at 0.1 mA to ensure that polysulfides were fully converted into solid Li₂S. Then, the batteries were potentiostatically charged at 2.35 V until the charge current is below 0.01 mA for completely dissolving Li₂S. Finally, the nucleation and dissolution capacity of Li₂S were evaluated by calculating the integral area of the curve drawn according to Faraday's Law.

Assembly of Li₂S₆ symmetric cells

Identical electrodes (FeSA-PCNF, PCNF and CNF) were assembled into CR2025 coin cells with 20 μ l Li₂S₆ electrolyte (0.2 M) in each cell. CV tests were performed on a CHI660E electrochemical workstation at 10 mV s⁻¹ within the potential range of -1 to 1 V.

Calculation of areal capacity and volumetric energy density

Areal capacity is calculated follow the equation:

$$Q_A = Q_0 \times L_{\text{sulfur}}$$

where Q_A is the corresponding areal capacity; Q_0 is the specific mass capacity, obtained directly from the Land battery test system, and L_{sulfur} refers to areal sulfur loading.

Volumetric energy density is calculated follow the equation:

$$E_{Vca} = \frac{Q_A}{d} \times U \text{ Wh L}^{-1}$$

where E_{Vca} is cathode-level volumetric energy density; d is the thickness of the cathode materials;

U is eclectic average voltage.

Density functional theory calculations

Density functional theory (DFT) calculations were carried out using the Vienna Ab initio Simulation Package (VASP) with the Perdew Burke-Ernzerhof (PBE) exchange-correlation potential within the generalized gradient approximation (GGA). A cutoff energy of 500 eV was

used for the plane-wave basis set. The convergence threshold was set to 10^{-5} eV in energy and 0.01 eV/Å in force, respectively. To prevent the interaction between two neighboring images, the vacuum layer thickness was set to 20 Å. A semi-empirical van der Waals (vdW) correction proposed by Grimme (DFT-D3) was included to account for the dispersion interactions. The binding strength of the surface adsorbate can be evaluated by the calculating of adsorption energy

(E_{ads}):

$$E_{\text{ads}} = E_{X^*} - E_X - E_*$$

where X , $*$, and X^* represent the adsorbate, substrate, and adsorption system, respectively.

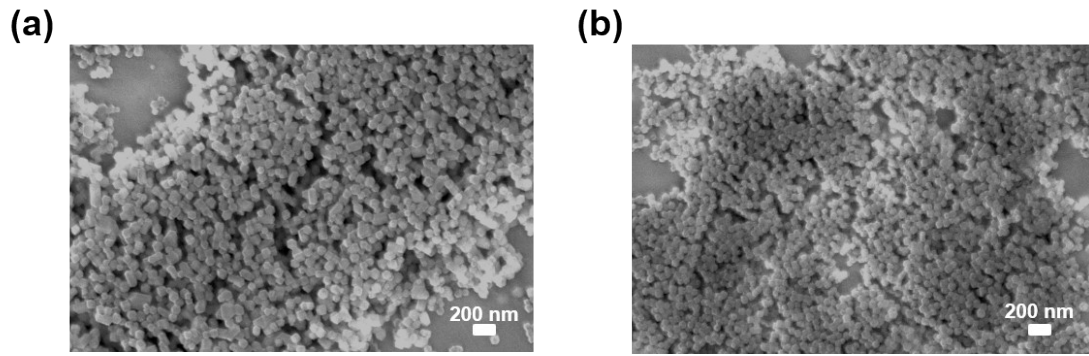


Figure S1. SEM images of (a) Fe-ZIF8 and (b) ZIF8.

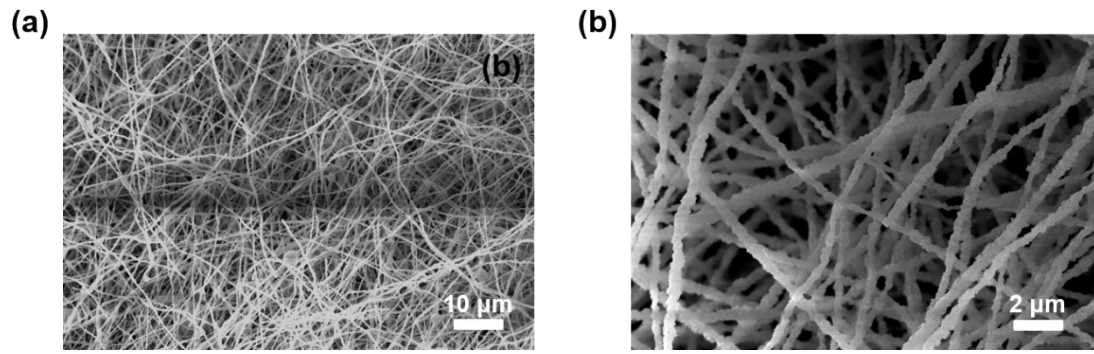


Figure S2. SEM images of PAN membrane precursor.



Figure S3. Digital images of (a) PAN membrane, (b) pre-oxidized membrane, (c) carbonized membrane and self-supported cathodes.

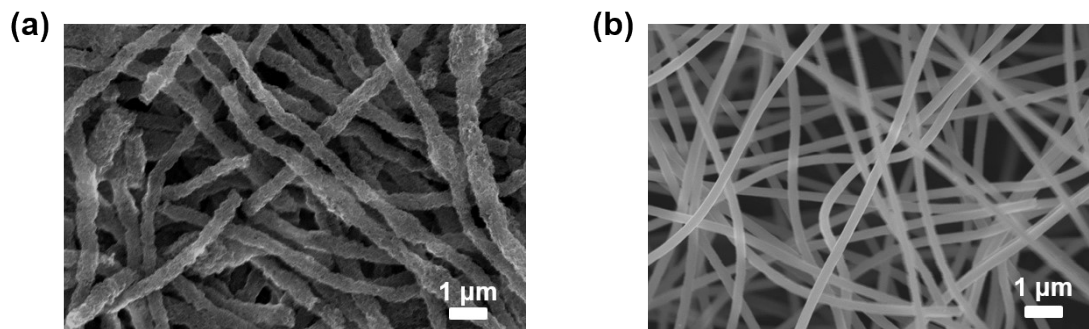


Figure S4. SEM images of (a) PCNF and (b) CNF.

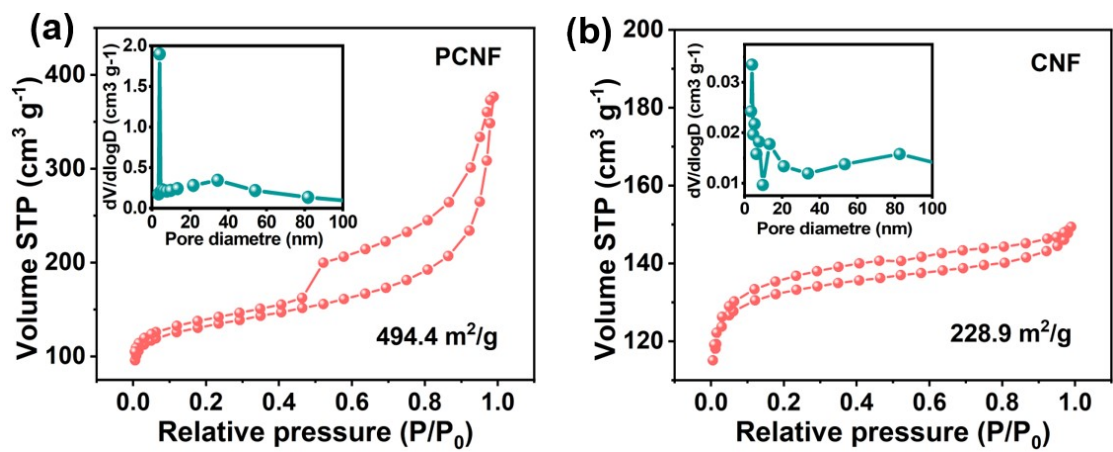


Figure S5. N_2 adsorption-desorption isotherms with the inset of pore distribution curves of (a)

PCNF and (b) CNF.

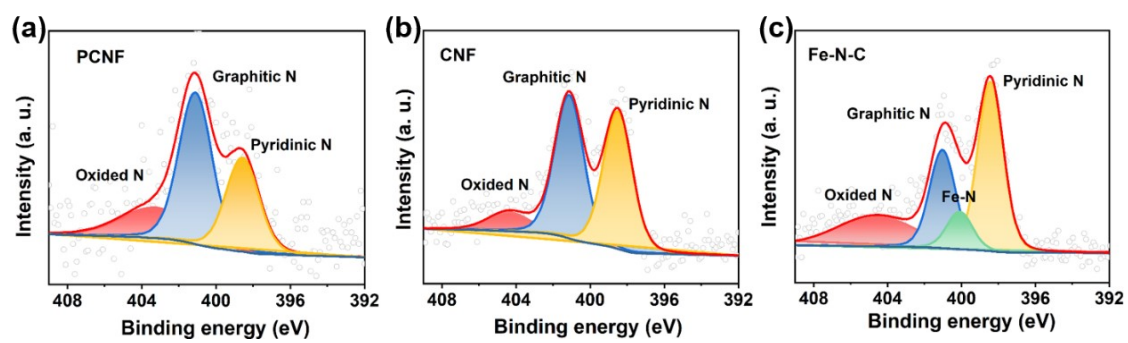


Figure S6. N 1s XPS spectra of (a) PCNF, (b) CNF, and (c) Fe-N-C.

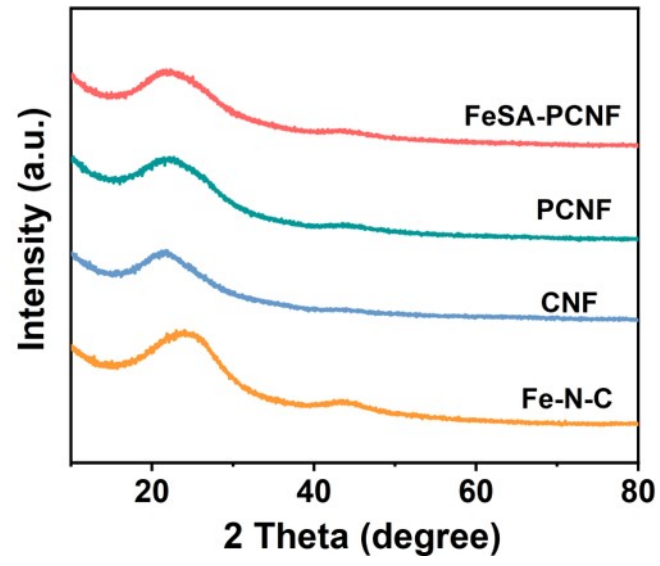


Figure S7. XRD patterns of different samples.

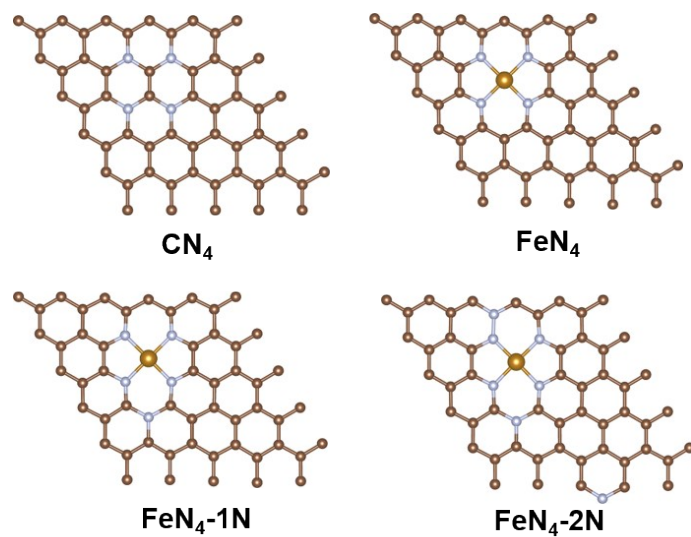


Figure S8. Atomic structure models of CN_4 , FeN_4 , $\text{FeN}_4\text{-1N}$ and $\text{FeN}_4\text{-2N}$.

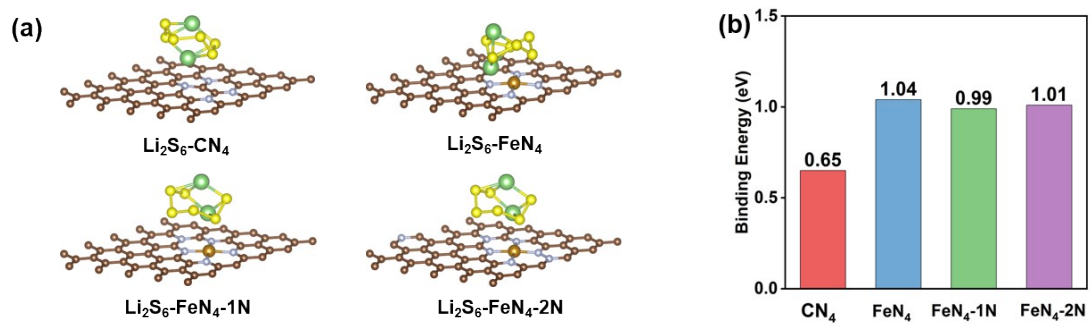


Figure S9. (a) Optimized structures of Li₂S₆ adsorption configurations on different sample surfaces and (b) the corresponding binding energies.

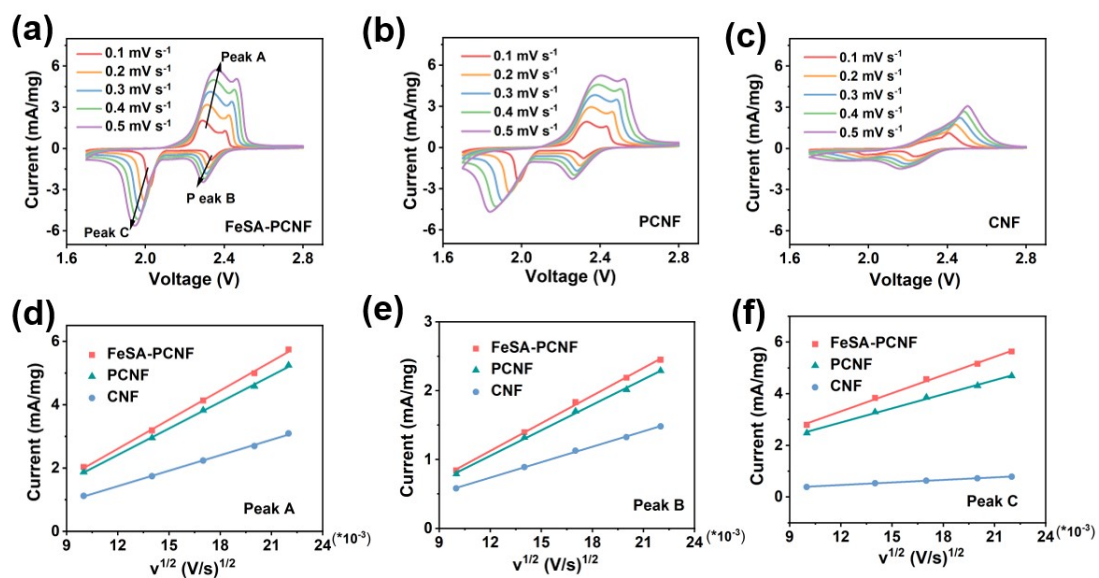


Figure S10. (a-c) CV curves of different cathodes at different scan rates from 1 to 5 mV s⁻¹. (d-f)

Corresponding linear fits of redox peak currents for Peak A, Peak B and Peak C.

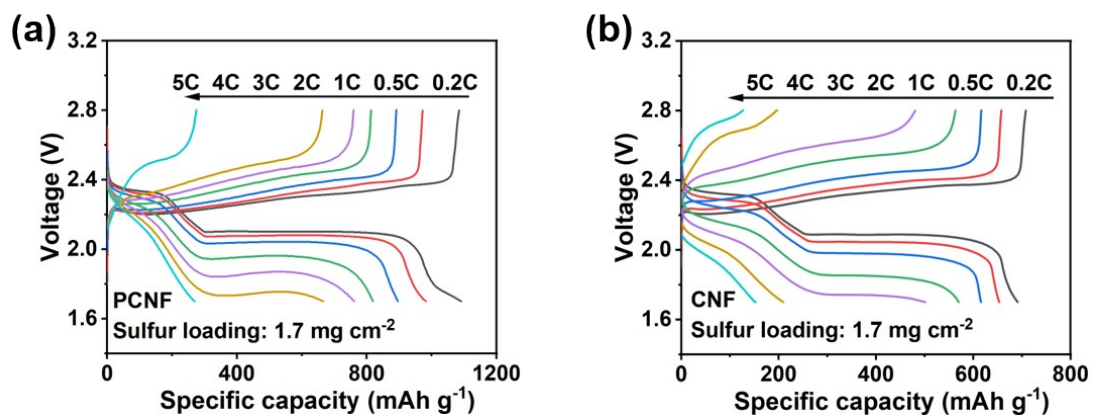


Figure S11. Voltage profiles of (a) PCNF and (b) CNF cathodes at different current rates.

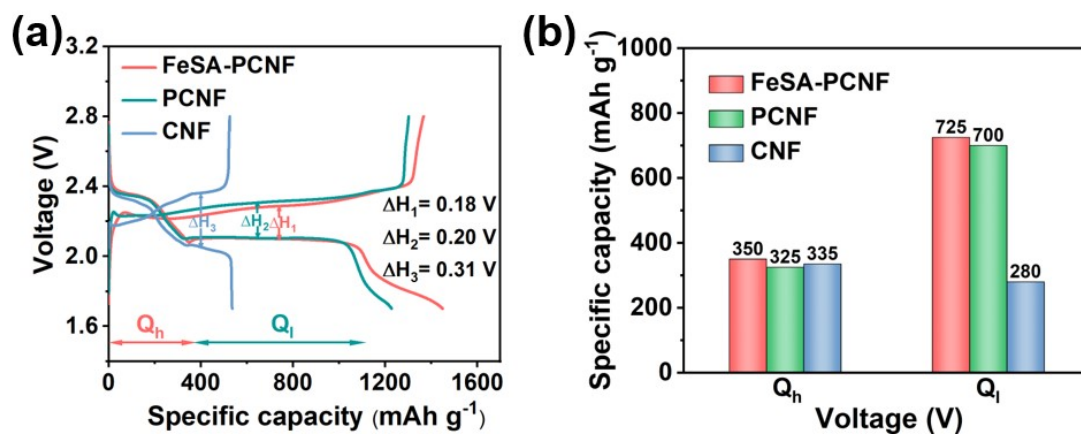


Figure S12. (a) Initial discharge/charge voltage profiles of different cathodes and (b) the comparison of discharge capacities at 0.2 C of FeSA-PCNF, PCNF, and CNF cathodes.

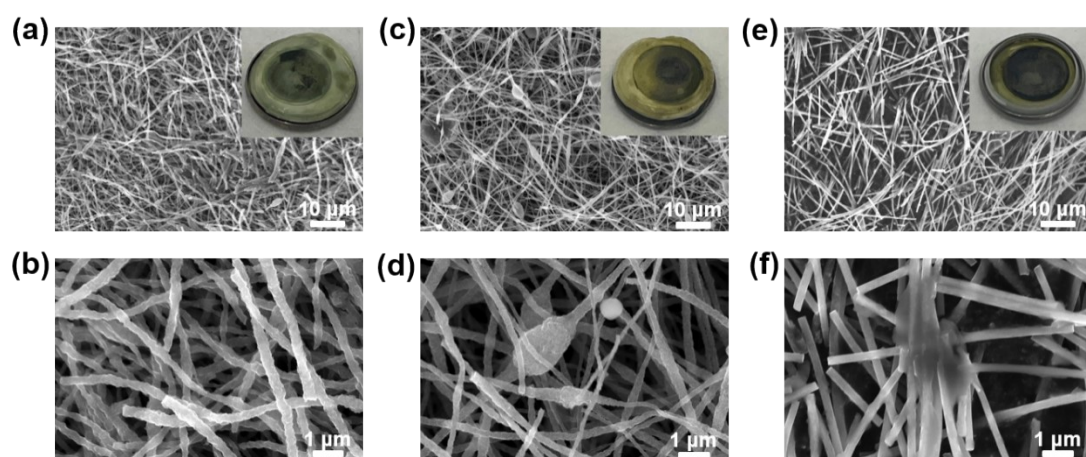


Figure S13. SEM images of (a, b) FeSA-PCNF, (c, d) PCNF, and (e, f) CNF electrodes after 100 cycles. The insets show the digital images of the corresponding separators.

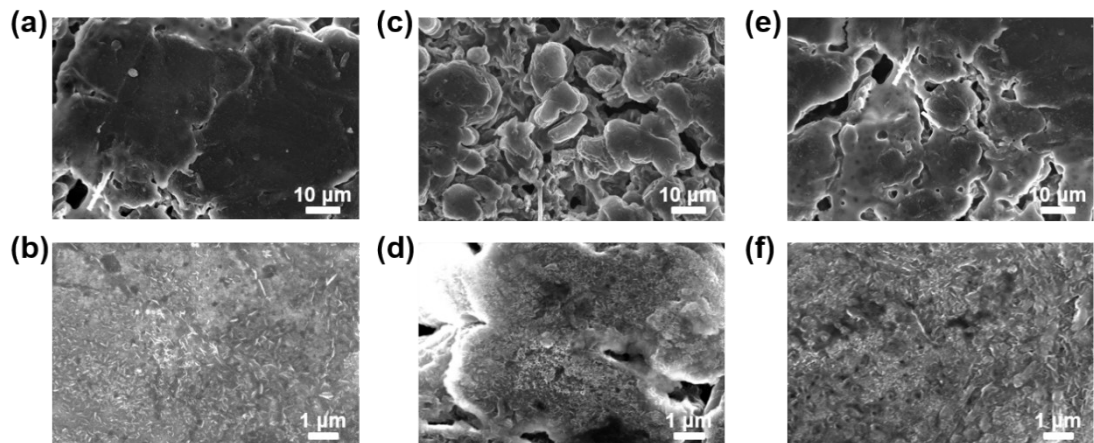


Figure S14. SEM images of Li anodes used for (a, b) FeSA-PCNF, (c, d) PCNF, and (e, f) CNF electrodes after 100 cycles.

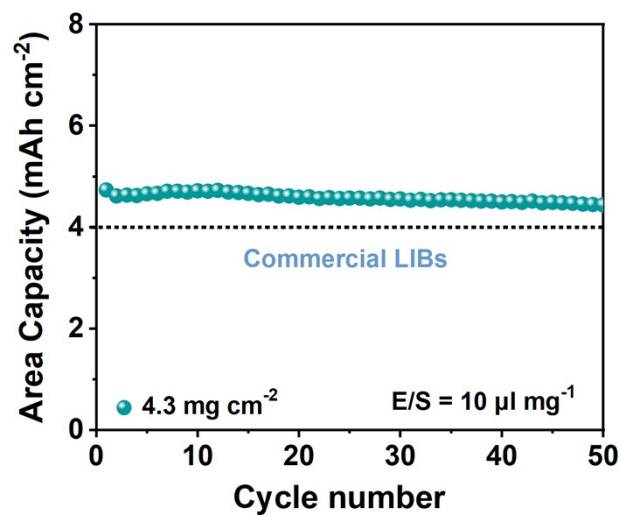


Figure S15. Cycling performance of FeSA-PCNF cathode with high sulfur loadings of 4.3 and 8.5 mg cm⁻² at 0.1 C.

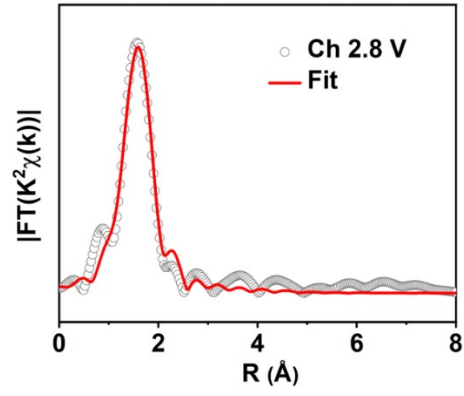


Figure S16. The corresponding fitting curve of EXAFS of FeSA-PCNF after charging to 2.8 V.

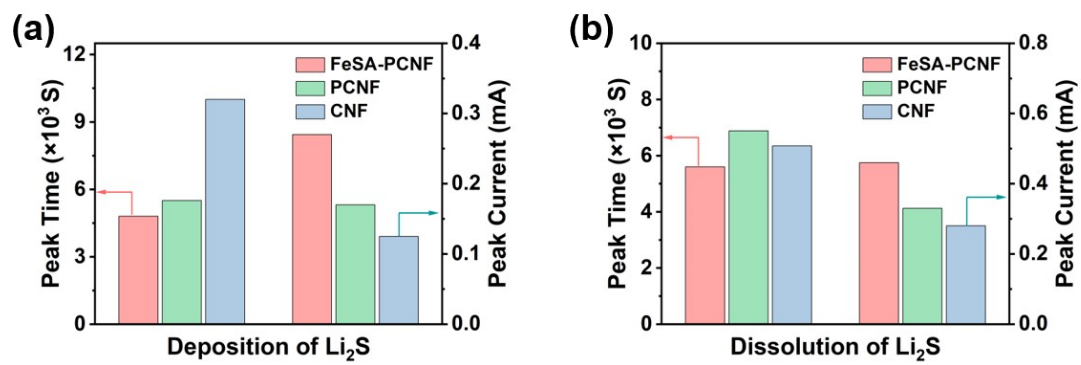


Figure S17. Comparison of peak times and peak currents during the (a) deposition of Li_2S and (b) dissolution of Li_2S processes.

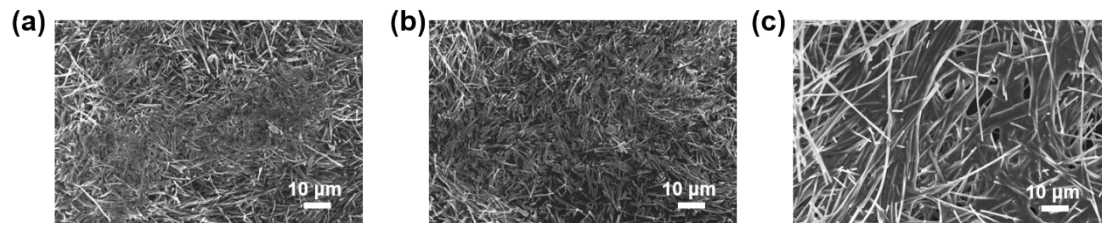


Figure S18. SEM images of (a) FeSA-PCNF, (b) PCNF and (c) CNF electrodes after Li_2S deposition measurements.

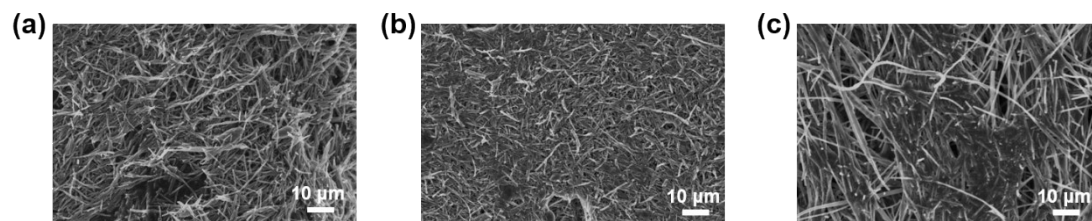


Figure S19. SEM images of (a) FeSA-PCNF, (b) PCNF and (c) CNF electrodes after Li_2S dissolution measurements.

Table S1. The ICP-OES results of FeSA-PCNF.

Element	Fe
Mass ratio (%)	0.78

Table S2. BET specific surface area, pore size, and pore volume of the three samples.

Samples	BET surface area (m² g⁻¹)	Pore size (nm)	Pore volume (cm³ g⁻¹)
FeSA-PCNF	669.5	5.67	0.96
PCNF	494.4	4.72	0.58
CNF	228.9	1.75	0.23

Table S3. EXAFS fitting parameters (R: bond distance; CN: coordination number; σ^2 : mean-square disorder; E_0 : energy shift).

Sample	Scattering Path	R (Å)	C.N.	σ^2	ΔE_0 (eV)
FeSA-PCNF	Fe-N	1.94	4.01	0.006	-4.48
	Fe-O	2.04	0.94	0.003	
Dch 2.1 V	Fe-N	1.94	4.00	0.016	-1.25
	Fe-S	2.24	1.59	0.003	
Dch 1.7 V	Fe-N	1.94	3.97	0.006	-4.06
Ch 2.8 V	Fe-N	1.94	3.56	0.013	0.18
	Fe-S	2.24	0.96	0.006	

Table S4. Comparison of single-atom-based sulfur hosts or electrospinning-based methods between this work and reported studies.

Materials	Sulfur loading (mg)	Area capacity (mAh cm⁻²)	Reference
FeSA-CN	6	5.1	J. Mater. Chem. A, 2020, 8, 3421-3430 ¹
Co-SAs@NC	5	5.5	Energy Storage Mater., 2020, 28, 196–204 ²
Fe-N ₅ -C	8.2	7.1	Angew. Chem. Int. Ed., 2021, 60, 26622-26629 ³
W/NC	8.3	8.7	Angew. Chem. Int. Ed., 2021, 60, 15563–15571 ⁴
Co-PCNF	6.9	7.1	ACS Nano, 2021, 15, 14105-14115 ⁵
HFeNG	6	4.5	Adv. Funct. Mater., 2018, 29, 1807485 ⁶
Co ₉ S ₈ @MoS ₂ /CNF	10	9.5	ACS Nano, 2020, 14, 17285-17294 ⁷
CPZC	9.2	8.1	Energy Environ. Sci., 2018, 11, 2372-2381 ⁸
FeSA-PCNF	17	11.1	This work

Reference

1. C. Wang, H. Song, C. Yu, Z. Ullah, Z. Guan, R. Chu, Y. Zhang, L. Zhao, Q. Li and L. Liu, *J. Mater. Chem. A*, 2020, **8**, 3421-3430.
2. Y. Li, G. Chen, J. Mou, Y. Liu, S. Xue, T. Tan, W. Zhong, Q. Deng, T. Li, J. Hu, C. Yang, K. Huang and M. Liu, *Energy Storage Mater.*, 2020, **28**, 196-204.
3. Y. Zhang, J. Liu, J. Wang, Y. Zhao, D. Luo, A. Yu, X. Wang and Z. Chen, *Angew. Chem. Int. Ed.*, 2021, **60**, 26622-26629.
4. P. Wang, B. Xi, Z. Zhang, M. Huang, J. Feng and S. Xiong, *Angew. Chem. Int. Ed.*, 2021, **60**, 15563-15571.
5. T. Huang, Y. Sun, J. Wu, J. Jin, C. Wei, Z. Shi, M. Wang, J. Cai, X. T. An, P. Wang, C. Su, Y. Y. Li and J. Sun, *ACS Nano*, 2021, **15**, 14105-14115.
6. Y. Wang, D. Adekoya, J. Sun, T. Tang, H. Qiu, L. Xu, S. Zhang and Y. Hou, *Adv. Funct. Mater.*, 2018, **29**, 1807485.
7. B. Li, Q. Su, L. Yu, J. Zhang, G. Du, D. Wang, D. Han, M. Zhang, S. Ding and B. Xu, *ACS Nano*, 2020, **14**, 17285-17294.
8. G. Li, W. Lei, D. Luo, Y. Deng, Z. Deng, D. Wang, A. Yu and Z. Chen, *Energy Environ. Sci.*, 2018, **11**, 2372-2381.